

Prospects of additional contribution at Optical-NIR band of EBL in the light of VHE spectra

Nijil Mankuzhiyil^{1*}, Massimo Persic^{2,3}, Alberto Franceschini⁴

¹ *Astrophysical Sciences Division, Bhabha Atomic Research Centre, Mumbai 400085, India*

² *INAF Osservatorio Astronomico di Padova, Vicolo dell'Osservatorio 5, I-35122, Padova, Italy*

³ *INFN-Trieste, via A.Valerio 2, I-34127 Trieste, Italy*

⁴ *University of Padova, Physics and Astronomy Department, Vicolo Osservatorio 3, I-35122 Padova, Italy*

Accepted XXX. Received YYY; in original form ZZZ

ABSTRACT

The Extragalactic Background Light (EBL) that spans the UV-IR band originates from direct and dust-reprocessed starlight integrated over the history of the Universe. EBL measurements are very challenging due to foreground emission like the zodiacal light and interplanetary dust emission. Indeed, some optical/NIR direct measurements overpredict EBL models based on galaxy counts. On the other hand, there is some debate on possible additional components of the Optical-NIR photon density: e.g., population-III stars, axion-photon decay, direct collapse of black holes, intra-halo light etc. Owing to the absorption of Very High Energy (VHE) γ rays by interaction with EBL photons, we study the prospects of accommodating an additional population of EBL sources in the Optical-NIR band on top of the standard galaxy-count-based component. To this aim we use 105 VHE spectra of 37 blazars with known redshifts, $0.03 < z < 0.94$. We correct the observed spectra for absorption by our model EBL. By requiring the intrinsic spectra to be non-concave and with a VHE spectral index > 1.5 , we estimate, at different wavelengths, upper limits to the additional low energy photon fields which would contribute to the absorption of γ -rays. Considering these limits we suggest that there is room for photons from Pop III stars and axion-like particle (ALP) annihilation. However, these additional hypothetical photon fields are bound to fall significantly below direct published EBL measurements by several instruments, and therefore our limits are either in tension or even inconsistent with such measurements.

Key words: galaxies: active – BL Lacertae objects: general – galaxies: distances and redshifts – gamma-rays: galaxies – stars: Population III

1 INTRODUCTION

The Extragalactic Background Light (EBL), that spans the UV-IR band, is the integrated diffuse starlight generated throughout the evolution of the Universe. Its spectral energy distribution (SED) consists of two humps: one arising from direct starlight that peaks at $\lambda \sim 1 \mu\text{m}$ (optical background), the other arising from dust-driven absorption of the UV starlight and reemission peaking at $\lambda \sim 100 \mu\text{m}$ (infrared background). Direct measurements of the EBL are hindered by foreground light, mostly the zodiacal light. Discrete sources like stars (primarily at ~ 1.25 to $3.5 \mu\text{m}$), scattered emission from interplanetary dust (at ~ 1.25 to $140 \mu\text{m}$), and interstellar dust (at $\geq 60 \mu\text{m}$) are also relevant sources of foreground light Hauser&Dwek (2001). Consequently, EBL measurements carry significant uncertainties (Matsuoka et al., 2011; Mattila et al., 2017) and indirect methods are banked upon in order to deduce the EBL photon density.

Galaxy evolution models may be used to determine the EBL SED at different redshifts. These models can be primarily classified as *forward evolution* and *backward evolution* models. The former

evolve galaxies in time from cosmological initial conditions using semi-analytical models of galaxy formation, stellar evolution, and dust-driven absorption/remission of photons [eg: Finke, Razzaque & Dermer (2010); Gilmore et al. (2012)]. The latter integrate the observed galaxy counts, which provide model-independent lower limits to the EBL, and are extrapolated to higher redshifts using number counts, redshift distributions, star formation rates, luminosity functions, or directly observed galaxy populations at different wavelengths [eg: Franceschini, Rodighiero & Vaccari (2008); Franceschini & Rodighiero (2017); Dominguez et al. (2011)].

On the other hand, even before extragalactic VHE γ -ray photons were detected an indirect method relying on Very High Energy (VHE; $E \gtrsim 30 \text{ GeV}$) observations of blazars was proposed to measure the EBL density (Stecker, de Jager & Salamon, 1992). This method relies on the concept that the interaction of VHE photons emitted by faraway sources with the intervening EBL leads to the formation of electron-positron pairs, $\gamma\gamma \rightarrow e^-e^+$. This results in an energy-dependent attenuation of the measured VHE flux. The first detections of VHE photons from Mrk 421 and Mrk 501 (by the Whipple and HEGRA telescopes respectively) yielded upper limits on the EBL density (Stecker, Salamon & Malkan, 1993; Stanev & Franceschini, 1998). Detections of relatively high- z

* E-mail: mankuzhiyil.nijil@gmail.com

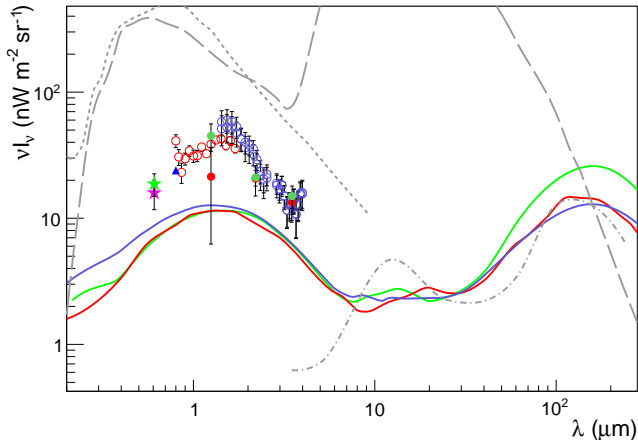


Figure 1. The predicted EBL intensity ($z=0$) versus wavelength by different models: Franceschini & Rodighiero (2017) (red), Gilmore et al. (2012) (blue), Dominguez et al. (2011) (green). Points correspond to recent EBL measurements in the optical-NIR band by various recent experiments. Open red circles: CIBER (Matsuura et al., 2017); open blue circles: IRTS reanalysis (Matsumoto et al., 2015); filled blue triangle: lower limit from the Hubble XDF (Matsumoto & Tsumuro, 2019); filled red circle: DIRBE (Levenson, Wright & Johnson, 2007); filled green circle: DIRBE (Sano et al., 2020); filled red and green stars: New Horizon (Lauer et al., 2021). The gray lines represent the major foregrounds (Leinert et al., 1998; Kashlinsky et al., 2005) in EBL measurements; dashed line: zodiacal light; dotted line: faint stars; dash-dotted line: cirrus.

blazars like H 2356-309 ($z = 0.165$), 1ES 1101-232 ($z = 0.186$) by HESS, 1ES 1011+496 ($z = 0.212$) by MAGIC, and PKS 1441+25 ($z = 0.939$) by VERITAS yielded plausible single-VHE-spectrum-based upper limit estimations on the EBL (Aharonian et al., 2006d; Ahnen et al., 2016b; Abeyskara et al., 2015). Modeling the optical-to-GeV SED of blazars, and comparing actual VHE data with the models extrapolated into the VHE range (where EBL absorption is effective), provides a way to estimate the actual EBL density at the source redshift (Mankuzhiyil, Persic & Tavecchio, 2010).

A larger set of blazar VHE spectra can lead to more robust estimates of the EBL. Mazin & Raue (2007) considered 13 observed VHE spectra to derive upper limits in the range $0.4\text{--}100\ \mu\text{m}$. Later Meyer et al. (2012) followed a similar approach using a sample of 23 VHE spectra together with the corresponding spectral parameters obtained from Fermi-LAT data. Biteau & Williams (2015), using 20 years of γ -ray observations, investigated the EBL and possible anomalies. Deducing 17 VHE spectra (H.E.S.S. data) of 7 blazars, Abramowski et al. (2013c) evaluated a normalization factor ~ 1.3 for the EBL optical depths of the Franceschini et al. (2008) model. Similarly, using 32 VHE spectra (MAGIC data) of 12 blazars Acciari et al. (2019c) estimated EBL optical depths, which turned out to be comparable, within factors of 0.82-1.23, to those of several EBL models. With a different approach, Abdalla et al. (2017) employed 19 VHE blazar spectra (H.E.S.S. data) with redshift $z < 0.29$ to estimate the EBL SED independent of existing EBL models.

2 AMBIGUITY IN THE OPTICAL-NIR PEAK

An excess population of EBL photon density (w.r.t. the estimated photon densities predicted by different EBL models and direct source counts) at $\sim 1\text{--}4\ \mu\text{m}$ was highlighted based on IRTS mea-

surements (Kashlinsky et al., 2004). Even though Mattila (2006) suggested this excess to be an artifact of improper zodiacal light subtraction, several subsequent measurements (by IRTS, HST, DIRBE, Spitzer, AKARI, New Horizons and CIBER) confirmed the excess – at $\sim 0.4\text{--}5\ \mu\text{m}$ [Matsuura et al. (2017); Sano et al. (2020); Lauer et al. (2021), and references therein]. This excess amounts to several times the predicted EBL based on different EBL models. For example, DIRBE measured an intensity of $45 \pm_{8}^{11}$ (at $1.25\ \mu\text{m}$), $21 \pm_{4}^{3}$ (at $2.2\ \mu\text{m}$), 15 ± 3 (at $3.5\ \mu\text{m}$) $\text{nWm}^{-2}\text{sr}^{-1}$, and CIBER indicates an intensity of $43 \pm_{11}^{12}$ $\text{nWm}^{-2}\text{sr}^{-1}$ (at $1.4\ \mu\text{m}$) – whereas model predictions are $\sim 1\ \mu\text{m}$ are $\sim 10\ \text{nWm}^{-2}\text{sr}^{-1}$ [eg: Finke et al. (2010); Gilmore et al. (2012); Franceschini & Rodighiero (2017); Dominguez et al. (2011)]. A New Horizons LORRI measurement at a distance of ~ 40 AU from the Earth (where the zodiacal light is very faint) measured a diffuse flux component of intensity 8.8 ± 4.9 to $11.9 \pm 4.6\ \text{nWm}^{-2}\text{sr}^{-1}$ at $0.4\text{--}0.9\ \mu\text{m}$, which is a factor 2 above the predicted EBL.

The measured optical-NIR excess, a few times larger than estimations through galaxy counts (see Fig. 1), may be an artifact from underestimating the zodiacal light (Driver et al., 2016) – but, on the contrary, it may be real and have an astrophysical origin. Population III (Pop-III) stars, which are primordial ($z > 6$), massive, metal-free stars, are a suitable candidate (Matsumoto et al., 2005; Kashlinsky et al., 2004). Considering the various uncertainties in Pop-III parameters (i.e., redshift, star formation rate) the estimation of their integrated emission is challenging. For example, for the optical peak Salvaterra & Ferrara (2003) estimated $\sim 60\ \text{nWm}^{-2}\text{sr}^{-1}$ whereas Sun et al. (2021), obtained a model estimate of $< 0.2\ \text{nWm}^{-2}\text{sr}^{-1}$. In the latter case, any signature of Pop-III stars in the EBL will be hardly noticed.

Decay of axion or axion-like particles (ALP) is another candidate to explain the HST and CIBER measurements between 0.6 and $1.6\ \mu\text{m}$, provided the axion mass is within $\sim 1\text{--}10\ \text{eV}$ (Gong et al., 2016). Direct collapse of a population of Compton-thick high- z black holes may also result in an excess EBL intensity of $\sim 1\ \text{nWm}^{-2}\text{sr}^{-1}$ at $\sim 2\ \mu\text{m}$ (Yue et al., 2013b). By using the LIGO black hole parameters Kashlinsky (2016) argued that a sufficiently large number of primordial black holes can result in an additional EBL source population at $2\text{--}5\ \mu\text{m}$. Recently, Lauer et al. (2021) justified the New-Horizons-measured unresolved EBL component invoking undetected $z > 6$ galaxies (assuming a steeper galaxy-count slope at $V > 24$, or a missing population of galaxies with $V < 30$).

After ruling out the arguments on the excess photons as originating from zodiacal light, diffuse Galactic light, known galaxies clustering, primordial galaxies, or black holes during cosmic reionization, Zemcov et al. (2014) associated the extra emission with intra-halo light (IHL), i.e. the emission from tidally stripped stars from their host galaxies at $z < 3$. On the contrary the spatial fluctuations of HST sky surveys at $0.6 < \lambda/\mu\text{m} < 1.6$, Mitchell-Wynne et al. (2015) dispense with the invoked extra populations of IHL-producing galaxies and $z > 6$ galaxies.

Hence, combining observations (from different instruments and background models) and phenomenological estimations, there clearly is an ambiguity in the optical-NIR band of the EBL, that leaves a possibility to accommodate an additional photon component of astrophysical origin. In what follows, we study this possibility using constraints derived by correcting observed VHE γ -ray spectra for the absorption due to an EBL model that consists of a baseline component (arising from galaxy counts) and an additional hypothetical component (of unspecified astrophysical origin).

AGN	Redshift	Reference
Mrk 421 (12 spectra)	0.031	1 - 7
Mrk 501 (17 spectra)	0.034	8 - 16
1ES 2344+514 (2 spectra)	0.044	17, 18
Mrk 180	0.045	19
1ES 1959+650 (5 spectra)	0.048	19 - 21
AP Librae	0.049	22
1ES 2037+521	0.053	23
PKS 0625-35	0.055	24
1ES 1727+501	0.055	25
PGC 2402248	0.065	26
PKS 0548-322	0.069	27
BL Lacertae (5 spectra)	0.069	28 - 31
PKS 2005-489 (2 spectra)	0.071	32, 33
RGB J0152+017	0.080	34
W Comae	0.102	35
1ES 1312-423	0.105	36
RGB J0521.8+211	0.108	37
PKS 2155-301 (13 spectra)	0.116	38 - 42
RGB J0710+591	0.125	43
H 1426+428	0.129	44
1ES 1215+202 (2 spectra)	0.131	45, 46
1ES 0806+524 (3 spectra)	0.138	47, 48
1ES 0229+200	0.140	49
IRXS J 101015.9-311909	0.143	50
H 2356-309 (4 spectra)	0.165	51, 52
RX J 0648.7+1516	0.179	53
1ES 1218+304 (3 spectra)	0.182	54 - 56
1ES 1101-232 (2 spectra)	0.186	57, 58
1ES 0347-121	0.188	59
RBS 0413	0.190	60
1ES 1011+496 (3 spectra)	0.212	61 - 63
1ES 0414+009 (2 spectra)	0.287	64, 65
PKS 1510-089 (5 spectra)	0.361	66 - 68
PKS 1222+216 (2 spectra)	0.432	69, 70
3C 279	0.536	71
B2 1420+32	0.682	72
PKS 1441+25 (3 spectra)	0.939	73, 74

Table 1. The data set used for this study. The columns are, the source name, redshift and reference numbers. The corresponding references are as follows: 1(Aleksic et al., 2012b) 2(Acciari et al., 2009b) 3(Aleksic et al., 2010) 4(Albert et al., 2007d) 6(Acciari et al., 2011b) 7(Abdo et al., 2011b) 8(Albert et al., 2007a) 9(Anderhub et al., 2009) 10(Acciari et al., 2011a) 11(Abdo et al., 2011a) 12(Acciari et al., 2020b) 13(Ahnen et al., 2017) 14(Aliu et al., 2016) 15(Aleksic et al., 2015b) 16(Aleksic et al., 2007e) 17(Allen et al., 2017) 18(Albert et al., 2006a) 19(Aliu et al., 2013b) 20(Acciari et al., 2020a) 21(Aliu et al., 2014) 22(Abramowski et al., 2015) 23(Acciari et al., 2020c) 24(Abdalla et al., 2018) 25(Archambault et al., 2015) 26(Acciari et al., 2019b) 27(Aharonian et al., 2010) 28(Albert et al., 2007c) 29(Arlen et al., 2013) 30(Abeysekara et al., 2018) 31(Acciari et al., 2019a) 32(Aharonian et al., 2005b) 33(Acero et al., 2010) 34(Aharonian et al., 2008) 35(Acciari et al., 2009a) 36(Abramowski et al., 2013a) 37(Archambault et al., 2013) 38(Aharonian et al., 2005a) 39(Aharonian et al., 2005c) 40(Abramowski et al., 2014) 41(Aharonian et al., 2009) 42(Abramowski et al., 2010a) 43(Acciari et al., 2010a) 44(Acciari et al., 2010b) 45(Aleksic et al., 2012a) 46(Aliu et al., 2013a) 47(Acciari et al., 2009d) 48(Aleksic et al., 2015a) 49(Aharonian et al., 2007a) 50(Abramowski et al., 2012a) 51(Aharonian et al., 2006b) 52(Abramowski et al., 2010b) 53(Aliu et al., 2011) 54(Albert et al., 2006b) 55(Acciari et al., 2009c) 56(Acciari et al., 2010c) 57(Aharonian et al., 2007c) 58(Aharonian et al., 2006c) 59(Aharonian et al., 2007b) 60(Aliu et al., 2012b) 61(Albert et al., 2007b) 62(Aleksic et al., 2016) 63(Ahnen et al., 2016a) 64(Abramowski et al., 2012b) 65(Aliu et al., 2012a) 66(Abramowski et al., 2013b) 67(Acciari et al., 2018) 68(Abdalla et al., 2021) 69(Aleksic et al., 2011a) 70(Ackermann et al., 2014) 71(Albert et al., 2008) 72(Acciari et al., 2021) 73(Abeysekara et al., 2015) 74(Ahnen et al., 2015)

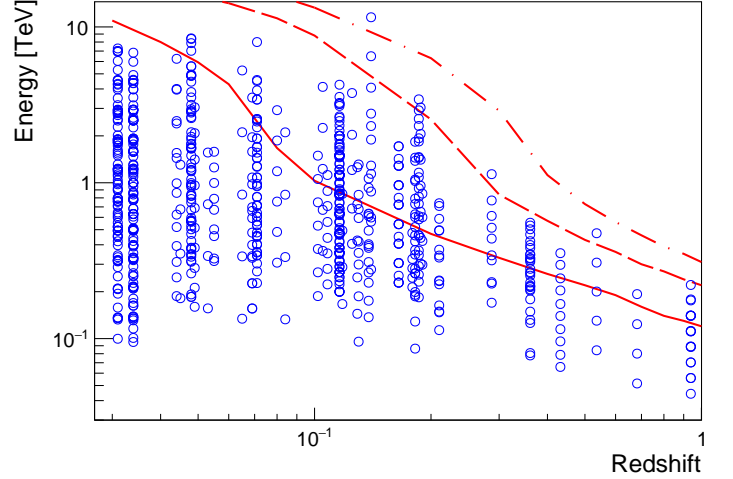


Figure 2. The energy vs. redshift distribution of the VHE spectral points considered in this study. The solid, dashed, and dot-dashed lines respectively correspond to the optical depths of $\tau = 1, 3,$ and 5 (Franceschini & Rodighiero, 2017).

3 DATA SETS

We have collected 105 VHE spectra from the major Imaging Atmospheric Cherenkov Telescopes (IACTs) in current operation, H.E.S.S. (Aharonian et al., 2006a), MAGIC (Aleksic et al., 2011b), and VERITAS (Weeks et al., 2002). These spectra correspond to 37 blazars and span the redshift range $0.03 < z < 0.94$. We limit our sample such that each spectrum should have at least 4 spectral points (in order to apply the method described below, see Section 4). Also, we do not include sources with unknown, indirect or disputed redshifts (e.g., PG 1553+113, 3C 66 A, PKS 1424+240, S5 0716+714). Considering their close proximity (hence, the negligible effect of the EBL on their observed spectra), the radio galaxies Centaurus A and M 87 are also not considered. The final sample of VHE spectra used in this study is given in Table 1. In Fig.2 we plot the datapoint energies against source redshift, and compare them with the optical depth of the Franceschini & Rodighiero (2017) EBL model.

4 METHOD

We choose the recent Franceschini & Rodighiero (2017) EBL model as our baseline model. This provides the *guaranteed* EBL density from galaxy number counts and luminosity functions. We further add different sets of Gaussian-shaped population components to the baseline model in $\log(\lambda)$ - $\log(\nu I_\nu(z))$ space (where λ is the observed EBL photon wavelength in μm , and $\nu I_\nu(z)$ is the EBL intensity at redshift z in $\text{nW m}^{-2}\text{sr}^{-1}$) at the optical-NIR peak, i.e.

$$F_{\text{add}} = B(z) \exp\left[-\frac{(x(z) - \mu(z))^2}{2\sigma^2}\right], \quad (1)$$

where $B(z)$ and $\mu(z)$ are normalization and mean wavelength (λ_m) in logarithmic scale of the additional component distribution, z is the redshift, σ is the standard deviation, and $x = \log(\lambda)$. We assume that the number density of this extra population increases with redshift as $(1+z)^3$. This factor takes care of the expansion of the Universe, under the assumption that the photon field originates from higher redshift than the VHE sources we considered. Since the astrophysical photon fields discussed in Section 2 are of high- z origin, this is a

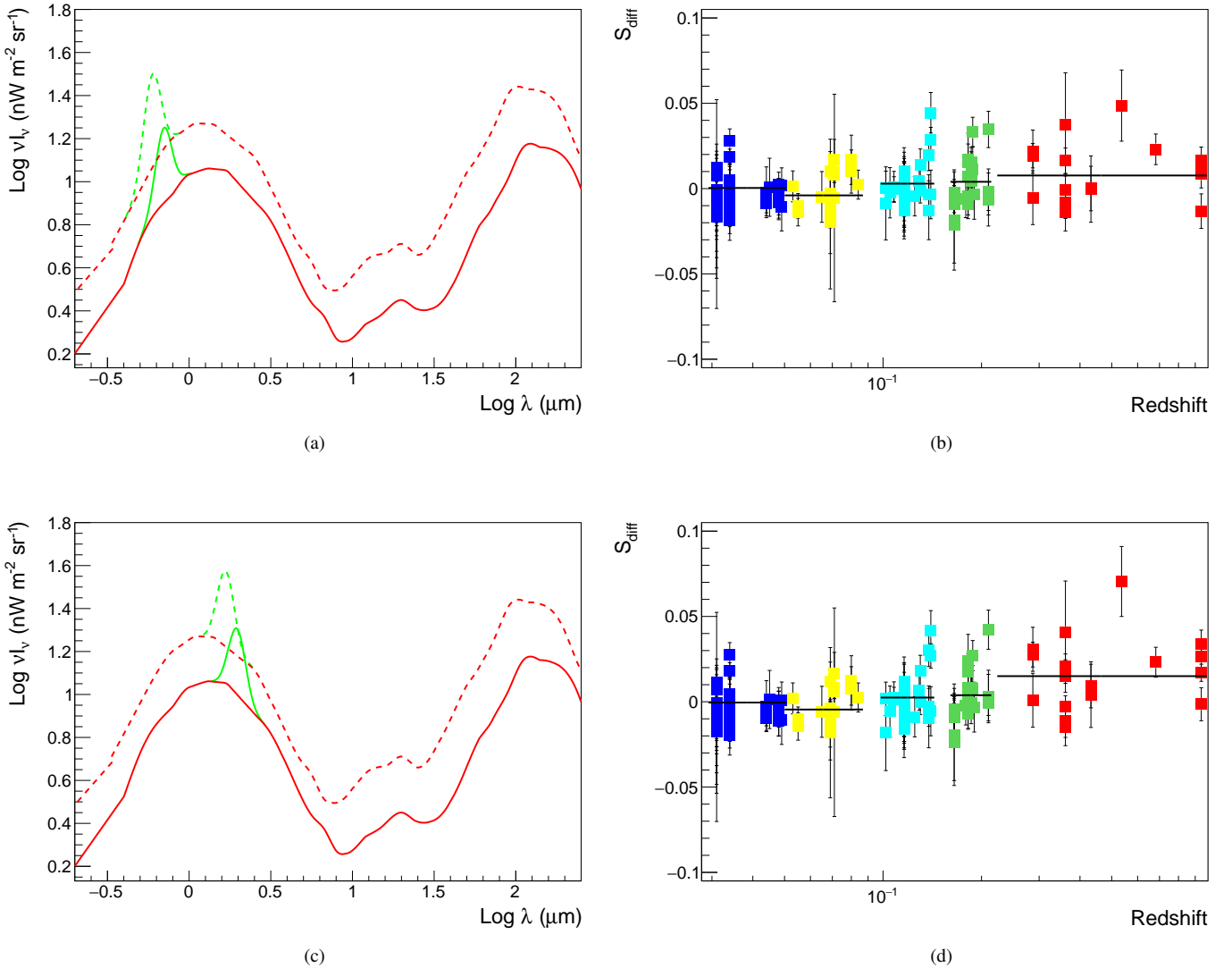


Figure 3. The baseline Franceschini & Rodighiero (2017) EBL model (red solid line), and the modified (baseline plus additional) EBL model (green solid line) at $z = 0$ in the optical-NIR band. The dashed lines represent the corresponding EBL at $z = 0.6$. *Left:* the additional component, of amplitude $10 \text{ nWm}^{-2} \text{sr}^{-1}$, is located at $0.71 \mu\text{m}$ (top) and $2.0 \mu\text{m}$ (bottom). *Right:* the corresponding distribution of the normalized difference S_{diff} (see Eq. 2) for the various redshift bands are shown ($0.00 < z \leq 0.05$: blue; $0.05 < z \leq 0.10$: yellow; $0.10 < z \leq 0.15$: cyan; $0.15 < z \leq 0.20$: green; $z > 0.25$: red).

reasonable assumption. To obtain optical depths at different spectral energies and redshifts, the resulting photon number densities (combination of the baseline EBL model and the Gaussian function population) are then integrated using Eq.(13) of Franceschini et al. (2008).

In order to segregate the acceptable additional population that can be accommodated on top of the baseline model, we scan the B , μ parameter space for a fixed value of σ . This operation is repeated for several values of σ . (Korochkin, Neronov & Semikoz (2019) adopted a similar approach employing γ -ray spectra of 7 blazars.)

As to the acceptance criteria for the excess populations, we adopt two approaches common in EBL studies when using VHE spectra. The first approach relies on the upward curvature of the de-absorbed VHE spectra of blazars (Mazin & Goebel, 2007; Horns & Meyer, 2012). Considering synchrotron radiation in the optical/X-ray band and Synchrotron-Self-Compton and External Compton emission in

the γ -ray band, concave VHE spectra are very unlikely. In order to quantify the spectral shape, we apply the new sets of EBL densities (i.e. the baseline model plus different extra populations) and fit the lower-energy spectrum (see next sentence) with a power-law shape ($\phi(E) \propto (E/E_0)^{-\alpha}$) or a Log Parabola shape ($\phi(E) \propto (E/E_0)^{-\alpha-\beta \ln(E/E_0)}$), in which $E_0 = \sqrt{E_{\text{min}} E_{\text{max}}}$ where E_{min} and E_{max} are the minimum and maximum photon energy in the VHE spectrum, α is the photon index, and β is the curvature parameter. We have then selected the fit which favours the lower reduced χ^2 values. We have also checked the dependence of the parameter E_0 by arbitrarily choosing different values, and found that this does not exert an appreciable difference to our results. More complex intrinsic spectral shapes (eg: power-law with an exponential cut off) were also considered. However, the F-test did not yield a statistically significant (95%) improvement of the fit results in such cases. Hence, complex functions (with more parameters) were not used in this study.

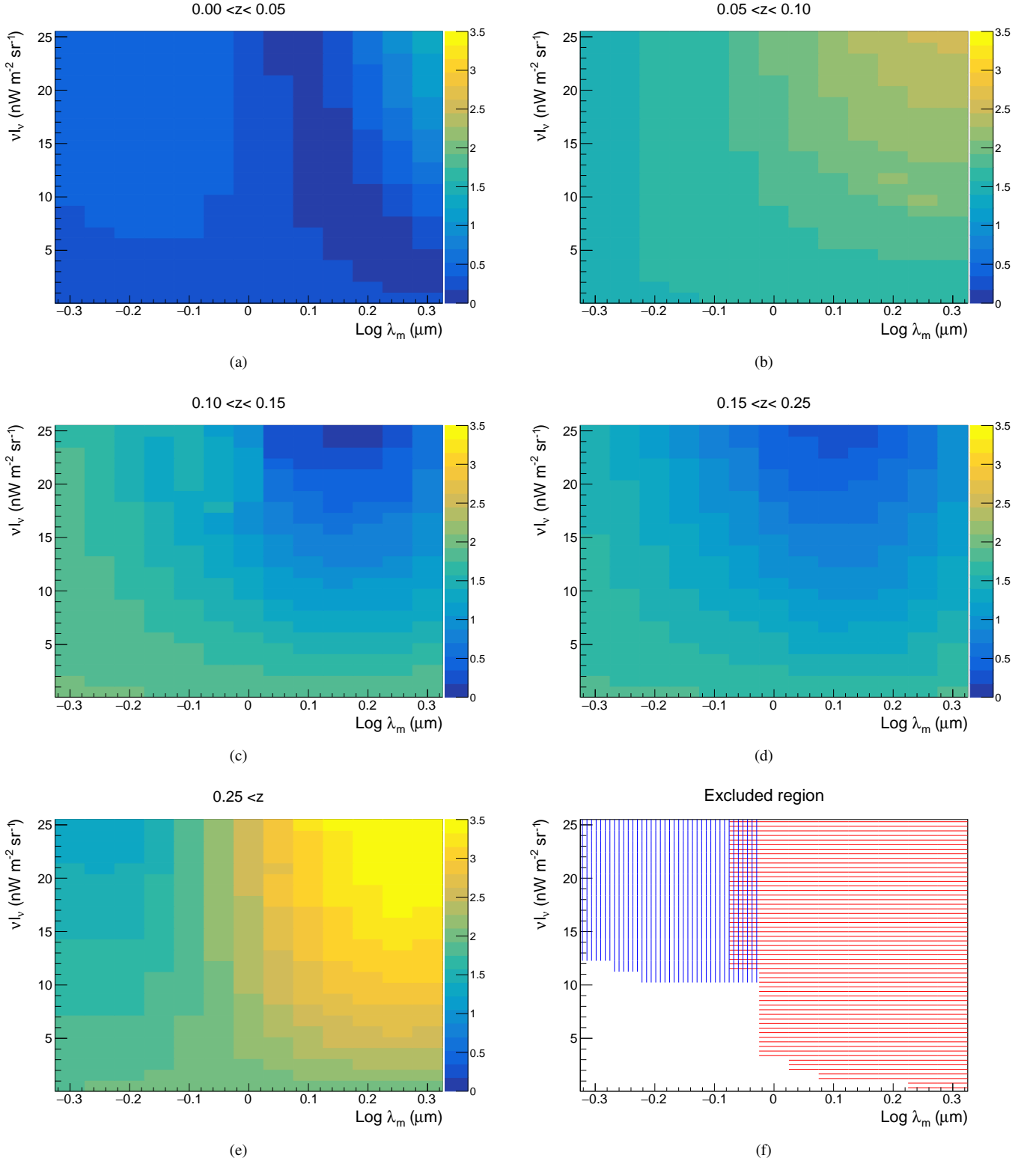


Figure 4. 2-D histograms ($z=0$) showing the t-value distribution when the additional component corresponds to different values of μ and B . The colours correspond to the t-values of each bins (see text also). The σ used in these plots is 0.05. The bottom-right figure is the combined image of all histograms. The red horizontal stripes region corresponds to p-value more than t_{95} , hence excluded based on the t-test. The blue vertical stripes correspond to the excluded region based on the spectral index $\alpha < 1.5$ of any spectrum. The white non-striped region is the resulting acceptable zone for $\sigma = 0.05$.

We extrapolate the fitted spectrum to the highest-energy point(s) – which was (were) not used for the fit. Such points are chosen as the last single point if the spectrum has ≤ 5 spectral points, or the last two points if the spectrum has > 5 points. We then estimate the difference between the flux at the highest-energy spectral point and the corresponding extrapolated flux. To avoid any bias arising from spectra of different flux levels, we normalize the differences obtained according to

$$S_{\text{diff}} = \frac{F_{\text{int}} - F_{\text{ext}}}{F_{\text{ext}} + F_{\text{int}}} \quad (2)$$

where F_{ext} is the extrapolated flux and F_{int} is the intrinsic flux at the highest energies. The resulting distribution after sampling S_{diff} in bins of different redshifts should ideally spread around 0 in the absence of any bias. The S_{diff} values from all the datapoints in different redshift bins are compared using the 'Student's T statistical test' (t-test). The null hypothesis for the t-test is that the differences are statistically not significant. If the null hypothesis is rejected, the corresponding EBL population (i.e., the baseline model plus the extra population) is ruled out.

The second approach relies on examining the derived intrinsic blazar VHE spectra in the light of standard particle acceleration constraints in both the leptonic and hadronic scenarios, i.e. the intrinsic spectral index is expected to be $\alpha > 1.5$ within error bars (Aharonian et al., 2006d; Mazin & Raue, 2007). Hence, we reject any extra component that gives rise to $\alpha < 1.5$, for any of the spectra.

5 RESULTS

The t-test values are calculated for the S_{diff} distribution in the redshift intervals 0.0-0.05, 0.05-0.10, 0.10-0.15, 0.15-0.25, and > 0.25 for several additional Gaussian-shaped EBL components. We first estimate the t-values of the distribution without adding any extra components. The t-values are 0.6, 1.6, 1.9, 1.8, and 1.6 with number of points 65, 20, 41, 25 and 17 in the redshift bands 0.0-0.05, 0.05-0.10, 0.10-0.15, 0.15-0.25, and > 0.25 . These values are below the 95% confidence level (i.e., t-values 2.0, 2.09, 2.02, 2.06, and 2.11 respectively). This indicates no significant evidence against the null hypothesis, i.e., the differences S_{diff} are not statistically significant (within 95% confidence level). We then calculate the t-test values after adding different Gaussian extra-populations to the baseline model.

For this, μ varies (by steps of 0.05) within -0.30 – 0.30 (corresponding to wavelengths $\lambda \sim 0.5$ – $2.0 \mu\text{m}$), and B varies by steps of $1 \text{ nWm}^{-2} \text{sr}^{-1}$ (after setting σ to a constant value¹) in order to obtain a total (model) EBL intensity at the optical-NIR peak of $\lesssim 35 \text{ nWm}^{-2} \text{sr}^{-1}$.

An example of S_{diff} distribution is given in Fig. 3 (b, d), with the corresponding EBL (Fig 3 a, c). The t-values obtained for each such combinations (with floating μ and B, and fixed $\sigma = 0.05$) at different redshift ranges are shown as 2-D histograms in Fig 4 (a, b, c, d, e). The obtained t-values in the lower-redshift samples do not significantly influence the rejection of extra-population EBL models. However, the t-value distributions for the high-redshift ($z > 0.25$) samples clearly tell the acceptable from the forbidden region (i.e., some specific extra-populations EBL models are not supported) in the μ -B plot. This is because of the strong cosmological increase, $\propto (1+z)^3$, of the additional population. Fig 4 (f) shows a combined image of

¹ Since the Gaussian spectrum is generated at high redshifts and photon energies and frequencies both scale as $(1+z)^{-1}$, σ is independent on redshift.

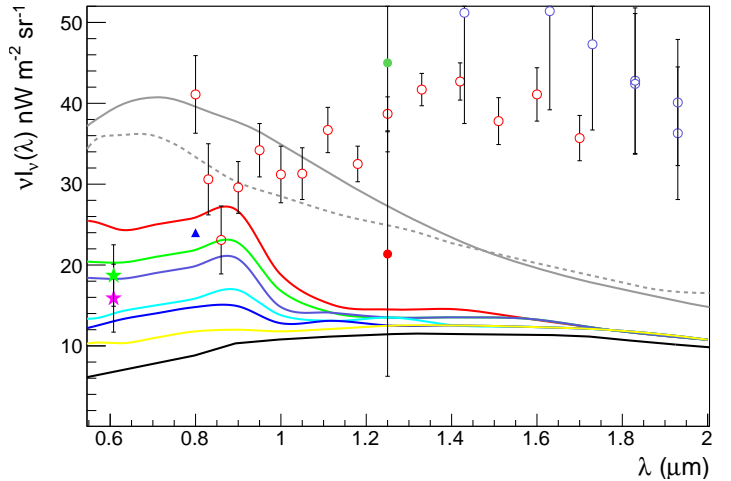


Figure 5. The obtained 95% confidence level upper limits on the amplitude of the Gaussian component (superposed on the baseline model) against optical-NIR wavelengths is shown as continuous lines. The red, green, violet, cyan, blue, and yellow lines correspond to the cases $\sigma=0.03, 0.04, 0.05, 0.07, 0.09$, and 0.12 , respectively. The black line denotes the baseline EBL model. Points representing EBL measurements are as in Fig. 1. We also show the upper limits obtained by Mazin & Raue (2007) and Meyer et al. (2012) in solid and dashed gray lines respectively.

the forbidden zone (with $\sigma = 0.05$) in our analysis: the horizontal red strips region shows the region excluded at 95% confidence level based on Student's t-test. We then check all the EBL-deabsorbed spectra for each set of extra-populations: models with μ and B values leading to a spectral index < 1.5 are ruled out: their region is denoted with vertical blue lines in Fig 4 (f). Hence, the acceptable combinations of μ and B (for $\sigma = 0.05$) are found in the non-shaded region of the figure.

Next we repeat the exercise considering Gaussian components with different σ 's starting from 0.03 (this can be considered very narrow, and corresponds to $\sim 4\%$ of the σ of the baseline-EBL's optical peak if the latter is roughly approximated with a Gaussian function) to 0.12, by intervals of 0.01. Clearly, the larger is σ the lesser is the possibility of adding an extra-population with a large amplitude to the existing EBL. For example, there is no room for a significant ($\gtrsim 1 \text{ nWm}^{-2} \text{sr}^{-1}$) Gaussian component for $\lambda > 0.89 \mu\text{m}$ if $\sigma = 0.12$. However, such a component with $\sigma = 0.03$ is permitted for $\lambda \leq 1.4 \mu\text{m}$. Similarly, only an extra-population of amplitude $1.1 \text{ nWm}^{-2} \text{sr}^{-1}$ can be accommodated at $0.79 \mu\text{m}$ for $\sigma = 0.12$, whereas a population contributing $\leq 18.7 \text{ nWm}^{-2} \text{sr}^{-1}$ at the same λ is admissible for $\sigma = 0.03$.

In Fig. 5 we show the obtained upper limits for the amplitude of the Gaussian component (Y-axis) if they were placed at different wavelengths (X-axis). As shown in the figure, assuming a narrow ($0.03 < \sigma < 0.12$) excess Gaussian components we rule out, with a confidence level of 95%, any significant (i.e., peak amplitude $> 1 \text{ nWm}^{-2} \text{sr}^{-1}$) additional population at $\lambda > 1.5 \mu\text{m}$.

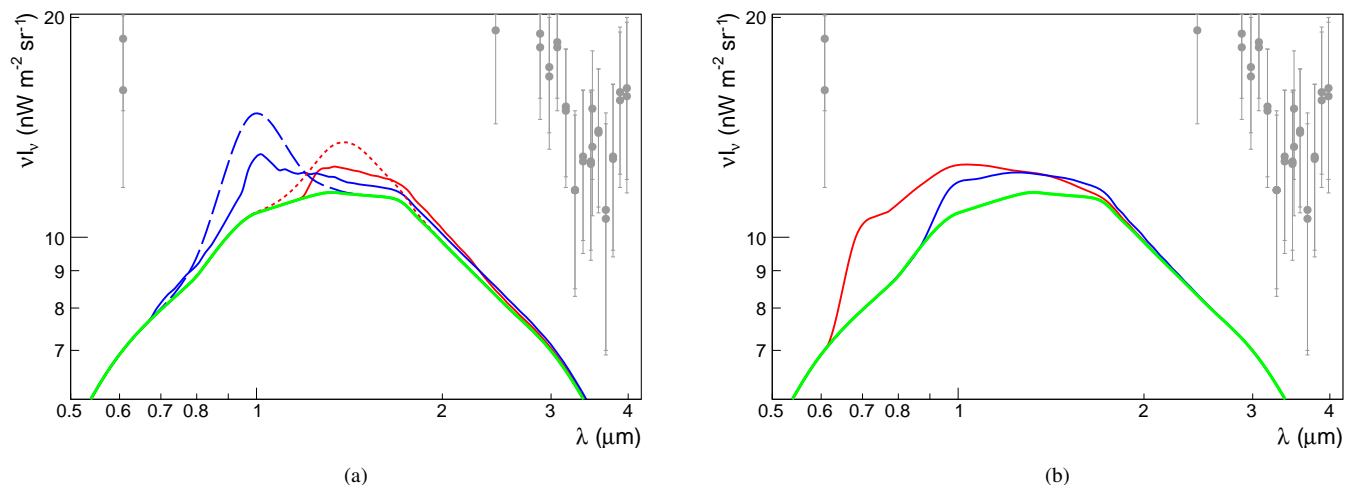


Figure 6. Examples of acceptable Pop-III models (on the left), and ALP annihilation models (on the right) together with the baseline EBL model (green solid line). The direct measurements below $20 \text{ nW m}^{-2} \text{ sr}^{-1}$ are shown in gray (see Fig. 1 for details). (a) The red line represents the modified (Salvaterra&Ferrara, 2003) model after scaling the original star formation efficiency down by a factor of 60, while the blue line shows the Fernandez et al. (2010) model after scaling the star formation efficiency down by a factor of 2. The dashed red and blue lines are the upper limits of Gaussian contribution (of $\sigma=0.05$) for comparison. Considering the wider distribution of the Pop-III model populations, the spectrum would be lower than Gaussian ULs. (b) Maximum allowed ALP annihilation component in the case of ALP mass $m_a=2.8 \text{ eV}$ (blue), and $m_a=4.0 \text{ eV}$ (red).

6 DISCUSSION

Our results are in conflict with recent estimations (at $\lambda \geq 1.2 \mu\text{m}$) by IRTS (Matsumoto et al., 2015), DIBRE (Sano, Kawara & Matsuura, 2016; Sano et al., 2020), AKARI (Tsamura et al., 2013), and CIBER (Matsuura et al., 2017). Our estimations also differ from the HST measurements (Kawara et al., 2017) at shorter wavelengths ($< 1 \mu\text{m}$), that anticipate an excess at a level of a few times the obtained upper limits. Recent measurements carried out by LORRI on-board the New Horizons satellite at a distance $>40 \text{ AU}$ from the Sun yielded an EBL intensity of 15.9 ± 4.2 to $18.7 \pm 3.8 \text{ nW m}^{-2} \text{ sr}^{-1}$ at $0.608 \mu\text{m}$ (Lauer et al., 2021). After subtracting contributions from known sources, the remaining excess is 8.8 ± 4.9 to $11.9 \pm 4.6 \text{ nW m}^{-2} \text{ sr}^{-1}$, in agreement with our estimates assuming excess components ($\sigma \leq 0.1$). The earlier LORRI estimates, that used data from limited observation time at $\sim 1.9 \text{ AU}$ distance from the Sun (Zemcov et al., 2017), also provided a 2σ upper limit on the EBL, $19.3 \text{ nW m}^{-2} \text{ sr}^{-1}$ at $0.65 \mu\text{m}$, which is well within our estimates. In Fig. 5 we also compare our estimates with recent direct measurements.

It is interesting to note that the results obtained from large samples of VHE spectra (Mazin & Raue, 2007; Meyer et al., 2012) are also in good agreement with our estimates, as they show a clear distinct peak at $\sim 0.7 \mu\text{m}$. Mazin & Raue (2007) predicts an upper limit of $40 \text{ nW m}^{-2} \text{ sr}^{-1}$, while Meyer et al. (2012) anticipates an upper limit of $24 \text{ nW m}^{-2} \text{ sr}^{-1}$. On the other hand, an additional peak was obtained by Korochkin et al. (2019) by employing the γ -ray spectra of 7 relatively nearby AGNs. The peak located at $\lambda = 1.7 \mu\text{m}$ with an amplitude of $15 \text{ nW m}^{-2} \text{ sr}^{-1}$ is in tension with our results. This could be due, to a large extent, to our advantage in using high- z blazar spectra.

The VHE spectra from blazars (especially FSRQs) are affected by internal absorption (Liu et al., 2008) due to multiple soft-radiation fields, mainly broad line region (BLR). However, considering different BLR parameters (size, thickness, temperature) Tavecchio & Mazin (2009) found no significant hardening in the IACT-accessible

VHE range – even in the extreme case of a UV radiation field (slope of $-1/3$), no $>60 \text{ GeV}$ spectral hardening is predicted. Since our high-redshift ($z > 0.25$) subsamples are dominated by FSRQs, it is important to validate our results in the light of internal absorption. Our high redshift data contains 4 spectral points below 60 GeV , hence we repeated the procedure by omitting these spectral points: we found no appreciable change in our results.

It is worth emphasizing that several studies [eg: (de Angelis et al., 2009; de Angelis, Galanti & Roncadelli, 2011; Meyer, Horns & Raue, 2013)] have suggested the possibility of γ -ray photon-ALP² oscillations in the presence of intergalactic magnetic fields. According to these models, the hardening or curvature of VHE spectra will be somewhat reduced by ALP oscillations. So in principle these hypothetical oscillations may potentially explain the differences between the direct measurements and the baseline EBL.

The redshifted light from Pop-III stars is often associated with the additional EBL population invoked for the Optical-NIR band (Kashlinsky et al., 2005). The peak of the Pop-III stars emission can be explained using the Ly α photons generated by reprocessing the UV photons in the ionized gas around the stars (Matsumoto et al., 2005; Fernandez & Zaroubi, 2013). Nevertheless, various models propose minute contribution (in which the peak of the spectra $P < 0.5 \text{ nW m}^{-2} \text{ sr}^{-1}$) from Pop-III stars [eg: Sun et al. (2021); Yue et al. (2013a); Fernandez & Zaroubi (2013); Inoue et al. (2013); Madau & Silk (2005)]. On the other hand, the models of Salvaterra&Ferrara (2003) reproduced direct NIR/EBL data peaking up to $\sim 70 \text{ nW m}^{-2} \text{ sr}^{-1}$ at $\sim 1-4 \mu\text{m}$. Those authors assumed three different star formation efficiencies f_* (defined as the fraction of baryons able to cool and form stars in a galaxy) for different assumptions

² Light ALP masses, $m_a \sim 10^{-10} - 10^{-6} \text{ eV}$, are relevant to the ALP-photon oscillation framework. On the other hand, heavy masses, $m_a \sim 1 - 10 \text{ eV}$, are relevant to the ALP-photon decay scenario (see section 2, and later this section).

of initial mass functions (IMF), by assuming a star formation cut-off $z_{\text{end}} \sim 8.8$. They essentially reproduce similar EBL densities ($f_* = 0.53, 0.21, \text{ and } 0.14$ for Salpeter, heavy and very heavy IMFs respectively), which are all clearly above the upper limit we set.

In the framework of the [Salvaterra&Ferrara \(2003\)](#) models, we modify the Pop-III spectra using lower f_* . An acceptable population (w.r.t. VHE spectra) is attained when the Pop-III contribution is scaled down by a factor of ~ 60 , i.e., 1.6% of the original star formation efficiency ($f_* \lesssim 0.008, 0.004, 0.002$ for Salpeter, heavy and very heavy IMFs respectively). The resulting Pop-III-derived photon spectrum is shown as red solid line in Fig. 6(a). Such a small peak is in good agreement with our results, considering that it is located at $>1 \mu\text{m}$. Moreover, the obtained Pop-III spectra, though not Gaussian shaped, is wider than the Gaussian spectral templates we assumed for the additional NIR photon fields: in this case the ULs shown in Fig. 5 are even more stringent. Arguably, then, a wider Pop-III contribution [eg: [Helgason et al. \(2016\)](#)] does not result in a significant difference in the measured flux versus estimates from galaxy counts.

In order to test a comparatively narrower Pop-III contribution together with our baseline EBL model, we adopted Pop-III spectra from [Fernandez et al. \(2010\)](#) which were derived using numerical simulations of reionization, a value of $f_* = 0.01$, and an IMF by [Larson \(1998\)](#). After applying such composite EBL to the VHE spectra, we reject this extra population at a confidence level of 95%. Scaling down the Pop-III spectrum by lower f_* values we derive an UL, $f_* \lesssim 0.005$, to the star-formation efficiency for the [Fernandez et al. \(2010\)](#) model: the resulting population is shown as a blue solid line in Fig. 6(a). We note that the peak of both (modified) Pop-III spectra in the figure are substantially lower than the directly measured fluxes. A narrower Pop-III contribution (i.e., strong Ly- α contribution w.r.t to the Pop-III continuum) will explain a significant difference between the observed flux and the estimated flux through galaxy counts. A larger Ly α bump indicates the presence of significant number of massive Pop-III stars at relatively lower redshifts [$z \lesssim 8$; [Fernandez & Zaroubi \(2013\)](#)].

Employing the UL from [Mazin & Raue \(2007\)](#) and different models of zero metallicity (ZM) and low metallicity (LM) stars, [Raue, Kneiske & Mazin \(2009\)](#) derived limits on the star formation rate (SFR), which is $\sim 0.3\text{-}3M_{\odot} \text{Mpc}^{-3} \text{yr}^{-1}$ in a redshift range of 7-14. In their study, they adopted a primordial stars EBL contribution of $5 \text{ nWm}^{-2} \text{sr}^{-1}$ at $\sim 2 \mu\text{m}$. Owing to a more restrictive upper limit ($\sim 1 \text{ nWm}^{-2} \text{sr}^{-1}$) we can estimate a SFR ~ 5 times lower than that of [Raue et al. \(2009\)](#) for a similar stellar population. However, considering the wider nature of their stellar EBL model, our estimate can be improved if we employ the stellar EBL densities superposed on the baseline EBL and estimate ULs. In order to prove this, we use 3 samples each for ZM and LM stars using different SFR parameters: ascending slope $\alpha=10$, descending slope $\beta=-2$, and peak redshift $z_{\text{peak}}=7, 10, 13$ (see, top panel of Fig. 6 in [Raue et al. \(2009\)](#) for details). We then estimate the SFR limits for this models, which turned out to be an order of magnitude lower than the original estimation. In Fig. 7 we show the modified SFR limits as a green shaded region, while the original limits are shaded in yellow. We also modify the SFR (corresponds to $f_* = 0.005$; see also table 3 of [Fernandez et al. \(2010\)](#)), which is shown as green solid line. Recent estimates of SFR from semianalytical models of the first stars ([Hartwig et al., 2022](#)) and cosmological simulations ([Sarmiento, Scannapieco & Cote, 2019](#); [Jaacks et al., 2018](#)) are also shown in the figure.

Axion (of mass $m_a \sim 1\text{-}10 \text{ eV}$) decay into Optical-NIR photons is also a potential source of EBL excess above $0.5 \mu\text{m}$. If single-mass axions are solely responsible for the significant excess [eg:

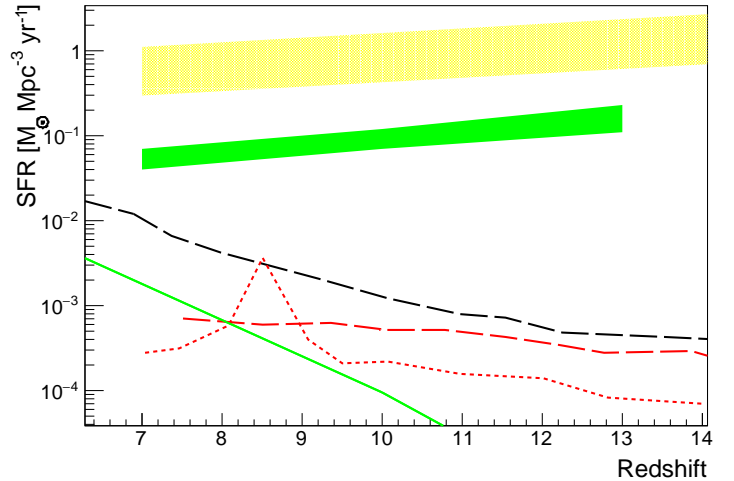


Figure 7. Co-moving SFR of ZM and LM stars obtained using 6 limited parameter samples (see text for details) in [Raue et al. \(2009\)](#) is shown as green shaded region, while the original estimation by [Raue et al. \(2009\)](#) is shown in yellow. The green line indicates the modified SFR for the adopted Pop-III model in [Fernandez et al. \(2010\)](#). Recent estimates from cosmological simulations and semianalytical models are also shown- black dash line: Pop-III+Pop-II ([Hartwig et al., 2022](#)); red dash line: Pop-III ([Sarmiento et al., 2019](#)) red dotted line: Pop-III ([Jaacks et al., 2018](#)).

[Caputo et al. \(2021\)](#)], combining the wide range of permitted m_a values and our UL (in which no substantial emission above $\sim 1.0 \mu\text{m}$ is allowed), we can estimate a lower limit on the axion mass of $m_a \gtrsim 2.5 \text{ eV}$ ([Gong et al., 2016](#)). However, if we consider a spectral distribution for the axion mass, the resulting intensity spectrum is significantly wider [eg: [Gong et al. \(2016\)](#)] and fall outside our estimated excluded region. To illustrate the case of ALP annihilation contribution to the EBL we employed Equation (4) of [Korochkin, Neronov & Semikoz \(2020\)](#). We have then repeated our analysis by varying the parameters of ALP mass (m_a) and two-photon coupling constant ($g_{a\gamma\gamma}$). As an example, see Fig. 6(b) in which the red line corresponds to the combination of $m_a=4.0 \text{ eV}$ and $g_{a\gamma\gamma}=1.6 \times 10^{-10}$, while the blue line refers to $m_a=2.8 \text{ eV}$ and $g_{a\gamma\gamma}=1.8 \times 10^{-10}$. After testing various parameter combinations we have estimated an acceptable zone (see Fig. 8) in the $m_a\text{-}g_{a\gamma\gamma}$ parameter space in which the ALP contribution does not fail the t-test. The favoured region obtained by [Korochkin et al. \(2020\)](#) contradicts our result because of the difference in basic assumptions of both approaches. They inferred no significant ALP contribution (hence, no extra bump, unlike it was shown in [Korochkin et al. \(2019\)](#)) to the baseline EBL, while we look for the maximum allowed ALP contribution to the baseline EBL. The lower limit of our acceptable zone refers to the ALP contribution peak of $1 \text{ nWm}^{-2} \text{sr}^{-1}$. We have also estimated a zone (red hatched region in Fig. 8) with which the ALP contribution exceeds the limit of acceptable EBL at different wavelength bands. The $m_a\text{-}g_{a\gamma\gamma}$ limits obtained under QCD framework (see [Anastassopoulos et al. \(2017\)](#) and references therein) is shown as gray band. The yellow band in the figure represents the limits obtained by the search of optical line emission from two-photon decay of axions ([Grin et al., 2007](#)).

Contributions from IHL ([Zemcov et al., 2014](#)) and faint galaxies ([Lauer et al., 2021](#)) result in wider spectra. Therefore, they do not yield a substantial deviation between the observed flux and estimates from galaxy counts. On the other hand, additional populations from

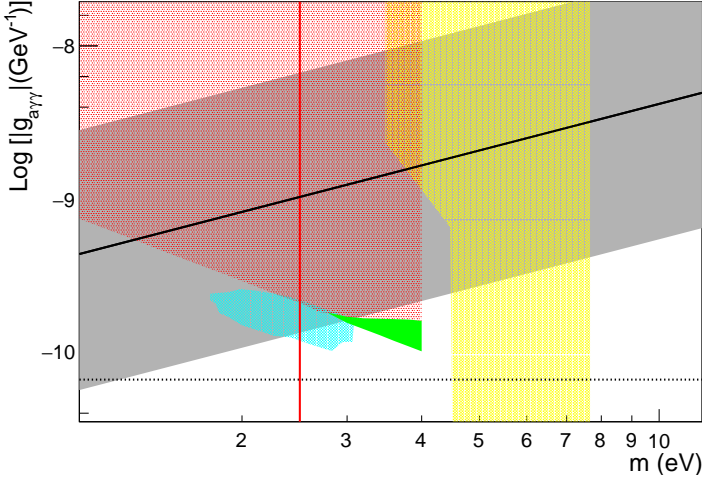


Figure 8. The obtained ALP-two photon coupling constraints. The green triangle shows the favored region between the maximum allowed contribution and a minimum significant contribution (ie, $\sim 1 \text{ nWm}^{-2} \text{sr}^{-1}$). The red hatched area is the region where a significant contribution to the EBL is excluded. The red vertical line corresponds to a mass $m_a = 2.5 \text{ eV}$ below which substantial ALP contribution to EBL is not favoured. The limits obtained from QCD models (gray shaded and black solid line), constraints obtained by observations of optical line emission from galaxy clusters (yellow hatched region), and non observation of excess energy loss in Horizontal Branch stars (dotted line) are also shown (see Anastassopoulos et al. (2017) and references therein, for details). The preferred region obtained by Korochkin et al. (2020) is shown in Cyan.

direct collapse of black holes and dark-matter-powered stars are not significant at $\lambda < 1 \mu\text{m}$ (Yue et al., 2013b; Maurer et al., 2012; Kashlinsky, 2016).

7 CONCLUSIONS

There is a large observational and phenomenological uncertainty concerning the Optical-NIR band of the EBL. Employing 105 VHE spectra of 37 blazars (with known redshift) and a baseline EBL model, we estimated an exclusion region in which an additional population of EBL sources may not be located. We have then compared it with recent direct EBL measurements and found that, at $\lambda \gtrsim 1 \mu\text{m}$, the latter exceed our ULs. The main conclusions of this paper can be summarized as follows.

1. Above $\lambda \gtrsim 1 \mu\text{m}$ no significant photon population can be accommodated on top of the baseline EBL model. This suggests the possibility that the direct measurements at $\gtrsim 1 \mu\text{m}$ may be affected by bad MilkyWay or zodiacal light subtractions.

2. The recent New Horizon measurements (Lauer et al., 2021) is well in agreement with our estimations. This may owe to the measurements being carried out at far distance from the Sun (beyond Pluto’s orbit), where zodiacal light is minimal.

3. Given the proposed frequencies and/or spectral widths of their photon population, we can rule out any significant (i.e., amplitude $\gtrsim 1 \text{ nW m}^{-2} \text{sr}^{-1}$) contributions from IHL, faint galaxies, direct black-hole collapse, dark-matter-powered stars, and annihilation of a spectral distribution of axion mass (Zemcov et al., 2014; Lauer et al., 2021; Yue et al., 2013b; Maurer et al., 2012; Kashlinsky, 2016; Gong et al., 2016).

4. There is room for considerable photon population from Pop-

III stars [(Salvatterra&Ferrara, 2003; Fernandez et al., 2010) with modified star formation rates] and ALP ($m_a > 2.5 \text{ eV}$) annihilation (Korochkin et al., 2020). However, these components, if they exist, would not saturate any existing differences between the published direct measurements and the baseline EBL density.

Since the high- z blazar spectra are suitable to determine the forbidden region for the extra population, low-energy-threshold VHE observations of distant blazars will be crucial in solving the ambiguity of Optical-NIR peak of the EBL. Direct measurements with space-borne instruments like JWST, CIBER-2, and upcoming missions like Euclid-LIBRAE, SPHEREx and WFIRST will also be relevant (Cheng&Chang, 2022; Kashlinsky et al., 2018) at clarifying the issue.

ACKNOWLEDGEMENTS

We acknowledge insightful comments and suggestions by the referee, Dr. Daniel Mazin, which have led to a substantial improvement of this paper.

DATA AVAILABILITY

The data of this work will be shared upon request to the corresponding author.

References

- Abdalla H. et al. 2021, A&A, 648, 23
 Abdalla H. et al. 2018, MNRAS, 476, 4187
 Abdalla H. et al. 2017, A&A, 606, 59
 Abdo A. A. et al. 2011a, ApJ, 727, 129
 Abdo A. A. et al. 2011b, ApJ, 736, 131
 Abeysekara A.U. et al. 2018, ApJ, 856, 14
 Abeysekara A.U. et al. 2015, ApJL, 815, 22
 Abramowski A. et al. 2015, A&A, 573, 31
 Abramowski A. et al. 2014, A&A, 571, 39
 Abramowski A. et al. 2013a, MNRAS, 434, 1889
 Abramowski A. et al. 2013b, A&A, 554, 107
 Abramowski A. et al. 2013c, A&A, 550, 4
 Abramowski A. et al. 2012a, A&A, 542, 94
 Abramowski A. et al. 2012b, A&A, 538, 103
 Abramowski A. et al. 2010a, A&A, 520, 83
 Abramowski A. et al. 2010b, A&A, 516, 56
 Ackermann M. et al. 2014, ApJ, 786, 157
 Acciari V.A. et al. 2021, A&A, 647, 163
 Acciari V.A. et al. 2020a, A&A, 638, 14
 Acciari V. A. et al. 2020b, A&A, 637, 86
 Acciari V.A. et al. 2020c, ApJS, 247, 24
 Acciari V.A. et al. 2019a, A&A, 623, 14
 Acciari V.A. et al. 2019b, MNRAS, 490, 2284
 Acciari V. A. et al. 2019c, MNRAS, 486, 4233
 Acciari V.A. et al. 2018, A&A, 619, 159
 Acciari V. A. et al. 2011a, ApJ, 792, 2
 Acciari J. et al. 2011b, ApJ, 738, 25
 Acciari V.A. et al. 2010a, ApJL, 715, 49
 Acciari V.A. et al. 2010b, ApJS, 247, 16
 Acciari V.A. et al. 2010c, ApJL, 709, 163
 Acciari V.A. et al. 2009a, ApJ., 707, 612
 Acciari V. A. et al. 2009b, ApJ, 703, 169
 Acciari V.A. et al. 2009c, ApJ, 695, 1370

- Acciari V.A. et al. 2009d, *ApJL*, 690c, 126
- Acero F. et al. 2010, *A&A*, 511, 52
- Aharonian H. et al. 2010, *A&A*, 521, 69
- Aharonian F. et al. 2009, *ApJL*, 696, 150
- Aharonian F. et al. 2008, *A&A L.*, 481, 103
- Aharonian F. et al. 2007a, *A&A L.*, 475, 9
- Aharonian F. et al. 2007b, *A&A*, 473, 25
- Aharonian F. et al. 2007c, *A&A*, 470, 475
- Aharonian F. et al. 2006a, *A&A*, 457, 899
- Aharonian F. et al. 2006b, *A&A*, 455, 461
- Aharonian F. et al. 2006c, *Nature*, 440, 101
- Aharonian F. et al. 2006d, *Nature*, 440, 1018
- Aharonian F. et al. 2005a, *A&A*, 442, 895
- Aharonian F. et al. 2005b, *A&A*, 436, 17
- Aharonian F. et al. 2005c, *A&A*, 430, 865
- Ahnen M. L. et al. 2017, *A&A*, 603, 31
- Ahnen M.L. et al. 2016a, *MNRAS*, 459, 2286
- Ahnen M. L. et al. 2016b, *A&A*, 590, 24
- Ahnen M.L. et al. 2015, *ApJL*, 815, 23
- Albert J. et al. 2008, *Science*, 320, 1752
- Albert J. et al. 2007a, *ApJ*, 669, 862
- Albert J. et al. 2007b, *ApJL*, 667, 21
- Albert J. et al. 2007c, *ApJL*, 666, 17
- Albert J. et al. 2007d, *ApJ*, 663, 1255
- Albert J. et al. 2007e, *ApJ*, 662, 892
- Albert J. et al. 2006a, *ApJL*, 648, 105
- Albert J. et al. 2006b, *ApJL*, 642, 119
- Aleksic J. et al. 2016, *A&A*, 591, 14
- Aleksic J. et al. 2015a, *MNRAS*, 451, 739
- Aleksic J. et al. 2015b, *A&A*, 573, 50
- Aleksic J. et al. 2012a, *A&A*, 544, 142
- Aleksic J. et al. 2012b, *A&A*, 542, 100
- Aleksic J. et al. 2011a, *ApJL*, 730, 8
- Aleksic J. et al. 2011b, *Astrop. Phys.*, 35, 435
- Aleksic J. et al. 2010, *A&A*, 519, 32
- Anastassopoulos V. et al. 2007, *Nature physics*, 13, 6
- Anderhub H. et al. 2009, *ApJ*, 705, 1624
- Aliu E. et al. 2016, *A&A*, 594, 12
- Aliu E. et al. 2014, *ApJ*, 797, 89
- Aliu E. et al. 2013a, *ApJ*, 779, 92
- Aliu E. et al. 2013b, *ApJ*, 775, 8
- Aliu E. et al. 2012a, *ApJ*, 755, 118
- Aliu E. et al. 2012b, *ApJ*, 750, 94
- Aliu A. et al. 2011, *ApJ*, 742, 127
- Allen C. et al. 2017, *MNRAS*, 471, 2117
- Archambault S. et al. 2015, *ApJ*, 808, 110
- Archambault S. et al. 2013, *ApJ*, 776, 69
- Arlen T. et al. 2013, *ApJ*, 762, 92
- Biteau J. & Williams D.A. 2015, *ApJ*, 812, 60
- Caputo A. et al. 2021, *JCAP*, 05, 46
- Cheng Y. & Chang T. 2022, *ApJ*, 925, 136
- Cooray A. et al. 2012, *Nature*, 490, 514
- de Angelis, Mansutti O., Persic M., Roncadelli M. 2009, *MNRAS*, 394, L21
- de Angelis, Galanti G. & Roncadelli M. 2011, *Phys. Rev. D*, 84, 105030
- Driver S.P. et al. 2016, *ApJ*, 827, 108
- Dominguez A., Primack J. R. & Rosario D. J. et al. 2011, *MNRAS*, 410, 4
- Fernandez E.R, Komatsu E., Iliev I. & Shapiro P.R. 2010, *ApJ*, 710, 1089
- Fernandez E.R & Zaroubi S. 2013, *MNRAS*, 433, 2047
- Finke J. D., Razzaque S., & Dermer C. D. 2010, *ApJ*, 712, 238
- Franceschini A., Rodighiero G., Vaccari M. 2008, *A&A*, 487, 837
- Franceschini A. & Rodighiero G. 2017, *A&A*, 603, 34
- Gilmore R. C., Somerville R. S., Primack J. R. & Dominguez A. 2012, *MNRAS*, 22, 4
- Gong Y. et al. 2016, *ApJ*, 825, 104
- Grin D. et al. 2007, *Phys. Rev. D*, 75, 105018
- Hartwig T. et al. 2022, *ApJ*, 936, 45
- Hauser M. G., Dwek E. 2001, *Annual Review of Astronomy and Astrophysics*, 39, 249
- Helgason K., Ricotti M., Kashlinsky A., Bromm V. 2016, *MNRAS*, 455, 282
- Horns D. & Meyer M. 2012, *JCAP*, 2, 33
- Inoue Y. et al. 2013, *ApJ*, 768, 197
- Jaacks J., Thompson R., Finkelstein S.L., Bromm V. 2018, *MNRAS*, 475, 4396
- Kashlinsky A., Arendt R., Gardner J. P., Mather J. C., & Moseley S. H., 2004, *ApJ*, 608, 1
- Kashlinsky A., Arendt R., Mather J. C. & Moseley S. H. et al. 2005, *Nature*, 438, 7064
- Kashlinsky A. 2016, *ApJL*, 823, 25
- Kashlinsky A. et al. 2018, *Rev. Mod. Physics*, 90, 025006
- Kawara K., Matsuoka Y., Sano K et al. 2017, *PASJ*, 69, 31
- Korochkin A., Neronov A., & Semikoz D. 2019, *A&A*, 633, 74
- Korochkin A., Neronov A., & Semikoz D. 2020, *JCAP*, 03, 64
- Lauer T. R. et al. 2021, *ApJ*, 906, 77
- Larson R.B. 1998, *MNRAS*, 301, 569
- Leinert Ch. et al., 1998, *A&AS*, 127, 1
- Levenson L.R., Wright E. L. & Johnson B.D., 2007, *ApJ*, 666, 34
- Liu H.T., Bai J.M. & Ma L. 2008, *ApJ*, 688, 148
- Madau P. & Silk J., 2005, *MNRAS*, 359, L37
- Mankuzhiyil N., Persic M. & Tavecchio F. 2010, *ApJL*, 715, 16
- Matsuoka Y., Ienaka N., Kawara K., Oyabu S. 2011, *ApJ*, 736, 119
- Matsumoto T. et al. 2005, *ApJ*, 626, 31
- Matsumoto T., Kim M. G., Pyo J., & Tsumura K, 2015, *ApJ*, 807, 57
- Matsumoto T. & Tsumura K, 2019, *Publ. Astron. Soc. Japan*, 71, 88
- Matsuura S. et al. 2017, *ApJ*, 839, 7
- Mattila K., 2006, *MNRAS*, 372, 1253
- Mattila K., Vaisanen P., Lehtinen K., von Appen-Schnur G., Leinert Ch. 2017, *MNRAS*, 470, 2152
- Maurer A., Raue M., Kneiske T. et al. 2012, *ApJ*, 745, 166
- Mazin D. & Goebel F. 2007, *ApJL*, 655, 13
- Mazin D. & Raue M. 2007, *A&A*, 471, 439
- Meyer M., Raue M., Mazin D. & Horns D. 2012, *A&A*, 542, 59
- Meyer M., Horns D. & Raue M. 2013, *Phys. Rev. D*, 87, 035027
- Mitchell-Wynne K. et al. 2015, *Nature Communications*, 6, 7945
- Raue M., Kneiske T. & Mazin D. 2009, *A&A*, 498, 25
- Salvaterra R. & Ferrara A. 2003, *MNRAS*, 339, 973
- Sano K., Kawara K. & Matsuura S. 2016, *ApJ*, 818, 72
- Sano K., Matsuura S., Yomo K., Takahashi A. 2020, *ApJ*, 901, 26
- Sarmiento R., Scannapieco E. & Cote B., 2019, *ApJ*, 871, 206
- Stecker F. W., Salamon M. H. & Malkan M. A. 1993, *ApJL*, 410, 71
- Stecker F. W., de Jager O. C. & Salamon M. H. 1992, *ApJ*, 390, 19
- Stanev T. & Franceschini A. 1998, *ApJ*, 494, 159
- Sun G., Mirocha J., Mebane R. H., Furlanetto S. 2021, *MNRAS*, 508, 1954
- Tavecchio F. & Mazin D. 2009, *MNRAS*, 392, L 40
- Tsumura K., Matsumoto T., Matsuura S., et al. 2013, *PASJ*, 65, 121
- Weeks T.C. et al. 2002, *Astrop. Phys.*, 17, 221

- Yue B., Ferrara A., Salvaterra R., Chen X. 2013a, MNRAS, 431, 383
Yue B., Ferrara A., Salvaterra R., Xu Y., Chen X. 2013b, MNRAS, 433, 1556
Zemcov M. et al. 2014, Science, 346, 6210
Zemcov M. et al. 2017, Nature Communications, 8, 15003

This paper has been typeset from a \TeX/L\AA\TeX file prepared by the author.